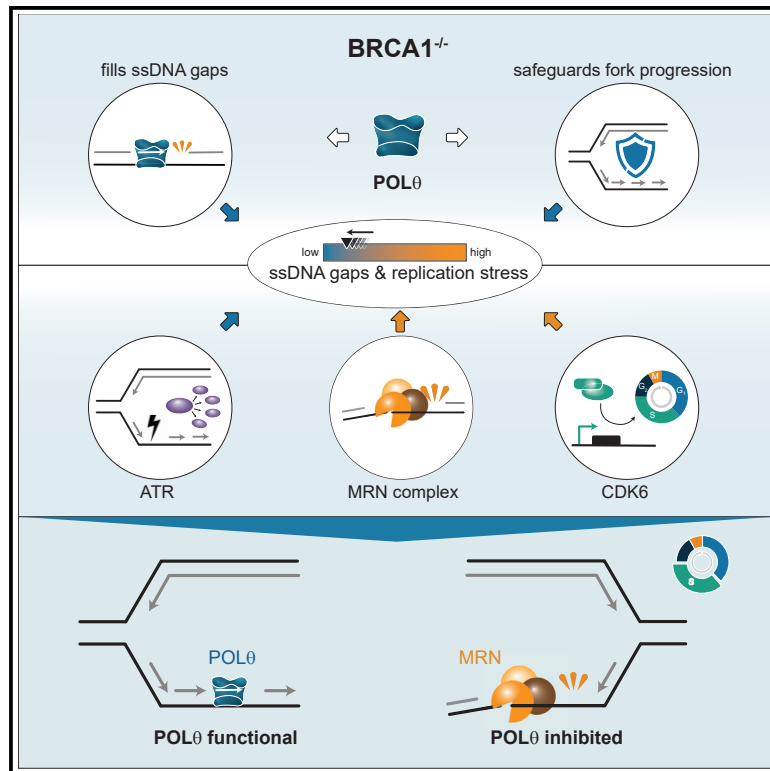


POL θ processes ssDNA gaps and promotes replication fork progression in BRCA1-deficient cells

Graphical abstract



Authors

Anna Schrempf, Sara Bernardo, Emili A. Arasa Verge, ..., Georg E. Winter, Vincenzo Costanzo, Joanna I. Loizou

Correspondence

joanna_loizou@hotmail.com

In brief

Schrempf and Bernardo et al. show that POL θ , known for its role in DNA double-strand break repair, is involved in filling single-stranded DNA gaps. This function becomes limiting in BRCA1-deficient cells, providing new insights into the genetic interaction between BRCA1 and POL θ that is currently exploited in clinical trials.

Highlights

- POL θ suppresses the formation of single-stranded DNA gaps
- POL θ suppresses replication stress, which is exacerbated upon BRCA1 deficiency
- The gap-filling activity of POL θ becomes limiting in BRCA1-deficient cells



Article

POL θ processes ssDNA gaps and promotes replication fork progression in BRCA1-deficient cells

Anna Schrempf,^{1,2,5} Sara Bernardo,^{1,5} Emili A. Arasa Verge,¹ Miguel A. Ramirez Otero,³ Jordan Wilson,^{1,2} Dominik Kirchhofer,¹ Gerald Timelthaler,¹ Anna M. Ambros,⁴ Atilla Kaya,⁴ Marcus Wieder,⁴ Gerhard F. Ecker,⁴ Georg E. Winter,¹ Vincenzo Costanzo,³ and Joanna I. Loizou^{1,2,6,*}

¹Center for Cancer Research, Comprehensive Cancer Centre, Medical University of Vienna, 1090 Vienna, Austria

²CeMM Research Center for Molecular Medicine of the Austrian Academy of Sciences, 1090 Vienna, Austria

³DNA Metabolism Laboratory, IFOM ETS, The AIRC Institute for Molecular Oncology, 20139 Milan, Italy

⁴Department of Pharmaceutical Sciences, University of Vienna, 1090 Vienna, Austria

⁵These authors contributed equally

⁶Lead contact

*Correspondence: joanna_loizou@hotmail.com

<https://doi.org/10.1016/j.celrep.2022.111716>

SUMMARY

Polymerase theta (POL θ) is an error-prone DNA polymerase whose loss is synthetically lethal in cancer cells bearing breast cancer susceptibility proteins 1 and 2 (*BRCA1/2*) mutations. To investigate the basis of this genetic interaction, we utilized a small-molecule inhibitor targeting the POL θ polymerase domain. We found that POL θ processes single-stranded DNA (ssDNA) gaps that emerge in the absence of BRCA1, thus promoting unperturbed replication fork progression and survival of BRCA1 mutant cells. A genome-scale CRISPR-Cas9 knockout screen uncovered suppressors of the functional interaction between POL θ and BRCA1, including NBN, a component of the MRN complex, and cell-cycle regulators such as CDK6. While the MRN complex nucleolytically processes ssDNA gaps, CDK6 promotes cell-cycle progression, thereby exacerbating replication stress, a feature of BRCA1-deficient cells that lack POL θ activity. Thus, ssDNA gap formation, modulated by cell-cycle regulators and MRN complex activity, underlies the synthetic lethality between POL θ and BRCA1, an important insight for clinical trials with POL θ inhibitors.

INTRODUCTION

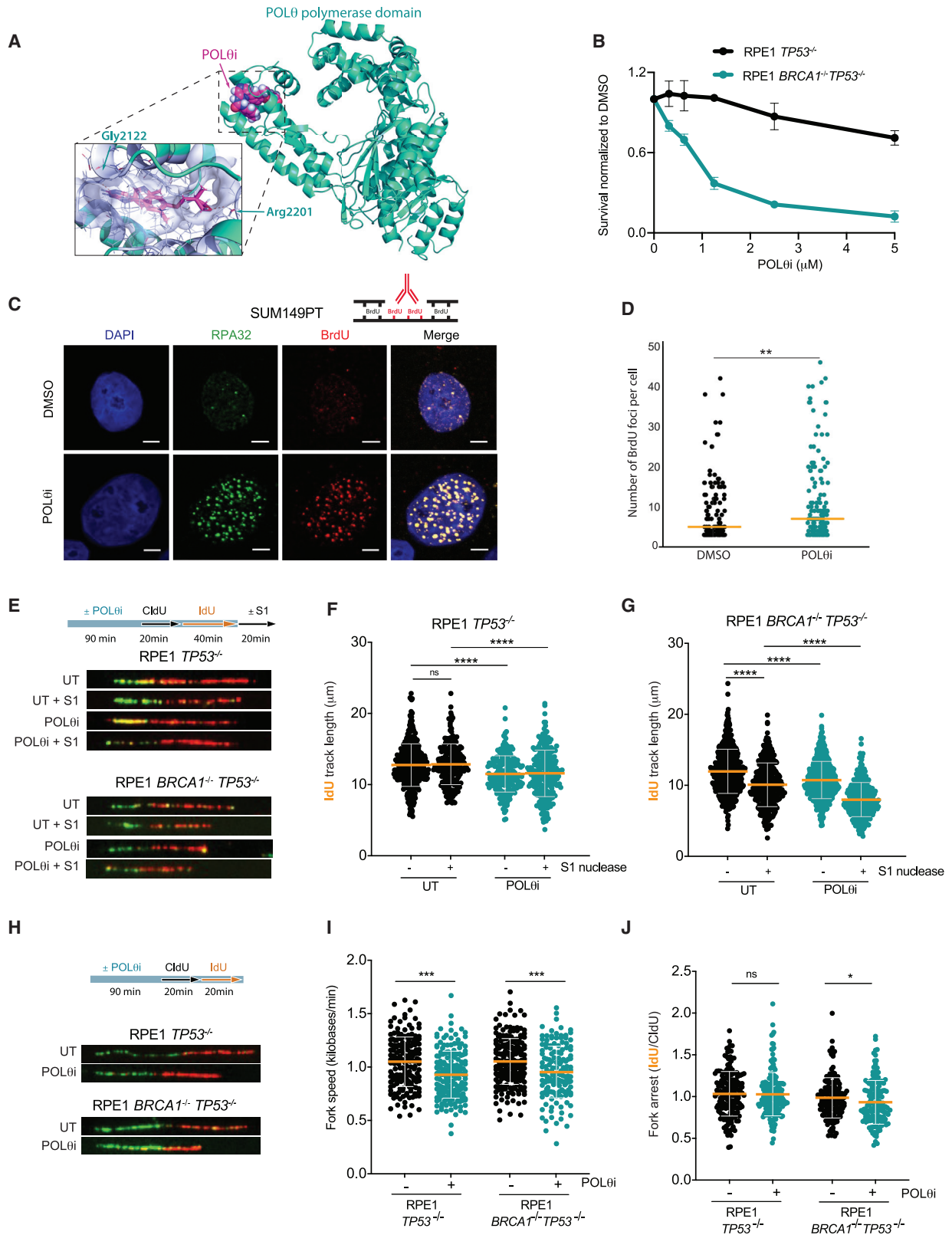
Mutations in breast cancer susceptibility proteins 1 and 2 (*BRCA1/2*) are the most common genetic predisposition associated with familial breast and ovarian cancer.¹ Thus, there is a growing interest in identifying synthetic lethal interactions of BRCA1/2 that can be exploited for targeted therapy, exemplified by the exquisite hypersensitivity of BRCA1/2-deficient cells to inhibitors of poly(ADP-ribose) polymerases (PARPs). BRCA1/2 function in homologous recombination (HR), a DNA double-strand break (DSB) repair pathway that utilizes the sister chromatid for precise repair. BRCA1/2 are indispensable for replication fork protection, a function that is independent of DSB repair.^{2,3} Specifically, these factors facilitate RAD51 loading onto nascent DNA, hence protecting stalled replication forks from collapse. In the absence of BRCA1/2, loss of RAD51 loading as well as unrestrained replication lead to the formation of single-stranded DNA (ssDNA).^{2,4–6} Recent lines of research have shown that such ssDNA regions are fundamental to the hypersensitivity of BRCA1/2-deficient cells to PARP inhibition.^{7,8} This can be explained by a role of PARP1 in sensing unprocessed Okazaki fragments that form during discontinuous replication of lagging

strands.⁹ Excessive ssDNA formation in cells lacking both PARP1 and BRCA1/2 activity ultimately exhausts cellular replication protein A (RPA), causing cell death by replication catastrophe.^{7,10,11} This suggests that replication gaps underlie BRCA deficiency and are fundamental to the response to PARP inhibitors.^{7,8,10}

Despite the clinical success of PARP inhibitors in the treatment of BRCA1/2 mutant cancers, the emergence of resistance is common, underlining the urgency to identify novel targets that can be exploited in resistant tumors.¹² In this context, the error-prone DNA polymerase polymerase theta (POL θ) has received considerable interest as a potential drug target.^{13,14} POL θ is a versatile enzyme that contains both a helicase and a polymerase domain. POL θ is involved in numerous DNA repair pathways including polymerase theta-mediated end joining (TMEJ), an error-prone pathway that seals resected DNA DSB ends, introducing characteristic microhomology-flanked deletions.¹⁵ Beyond DSB repair, POL θ functions as a translesion synthesis polymerase to process helix distorting lesions such as those generated by UV radiation.¹⁶

The genetic interaction between BRCA1 and POL θ is believed to be a result of their converging roles in DNA DSB repair.^{13,14}





(legend on next page)

Resected DNA DSBs, which cannot be processed by HR in the context of BRCA1/2 deficiency, are thought to be processed by POL θ -dependent TMEJ. The dependency on TMEJ in HR-deficient cells has contributed to the interest in POL θ as an anti-cancer target.¹⁷ Recently, two first-in-class POL θ inhibitors (POL θ i)s with *in vivo* efficacy have been reported that potentially represent a valuable therapeutic approach for the treatment of BRCA1/2-deficient cancers.^{18,19} However, although ssDNA gaps are now considered to be the major lesions that drive cell death in BRCA1/2-deficient cells treated with PARP inhibitors or cisplatin, it remains unclear whether ssDNA formation contributes to the genetic interaction between BRCA1/2 and POL θ .

In this study, we show that loss of POL θ activity in the context of BRCA1 deficiency exposes ssDNA, which causes replication stress and deregulation of S-phase progression. In a genome-wide CRISPR-Cas9 knockout (KO) screen, we uncover modulators of the functional interaction between BRCA1 and POL θ including the MRN complex and the cycle regulator CDK6. We find that the MRN and CDK6 activity promote POL θ i-induced DNA damage by two distinct cellular processes. Loss of MRN-complex activity suppresses nucleolytic processing of gaps, whereas CDK6 loss reduces replication stress by diminishing entry into S-phase. Thus, we define a role for POL θ in suppressing the accumulation of ssDNA gaps, a hallmark that is fundamental to its synthetic lethality with BRCA1, and uncover molecular factors that modulate this interaction.

RESULTS

POL θ processes ssDNA gaps generated in BRCA1-deficient cells

Although loss of POL θ activity is known to be synthetic lethal with BRCA1 deficiency, the basis of this genetic interaction is not fully understood.^{13,14} To address this question, we used a small-molecule inhibitor of POL θ (termed POL θ i) based on the structures of a recently published POL θ i patent family²⁰ (Figure S1A). Through computational docking, we show that the POL θ i binds to an allosteric pocket in the thumb subdomain of

POL θ (Figure 1A) and subsequently inhibits its polymerase activity.²¹ We tested the inhibitor using an isogenic pair of p53 mutant human TERT-immortalized retinal pigment epithelial 1 (RPE1) cells deficient or proficient for BRCA1 (denoted RPE1 *BRCA1*^{-/-} *TP53*^{-/-} and RPE1 *TP53*^{-/-}, respectively) (Figures S1B and S1C). As expected, the BRCA1-deficient cells were hypersensitive to increasing concentrations of POL θ i compared with their BRCA1 wild-type counterparts (Figures 1B and S1D). In addition, POL θ i increased the sensitivity of RPE1 *TP53*^{-/-} cells to the DSB-inducing agent etoposide in a dose-dependent manner, in line with POL θ functioning in DSB repair (Figure S1F).

The accumulation of ssDNA gaps has been reported in BRCA1-deficient cells.^{5,7,9,10} While it is known that PARP1 signals the presence of these gaps,⁹ the processing steps that lie downstream of this signaling are still under debate. To determine if loss of POL θ activity affects the processing of ssDNA gaps in BRCA1-deficient cells, we utilized the triple negative breast cancer cell line SUM149PT, which harbors a hemizygous BRCA1 frameshift mutation resulting in a partially defective BRCA1 protein and hypersensitivity to PARP and POL θ inhibition (Figures S1B–S1E). To visualize ssDNA, cells were pre-labeled with the nucleoside analogue BrdU, which was detected by immunofluorescence under native conditions. When making the entire genome accessible to the BrdU antibody by denaturing the cells prior to immunofluorescence, the BrdU signal was dramatically increased, providing a quality control for the robust integration of a nucleoside analog (Figure S1G). Under native conditions, we observed elevated ssDNA levels following POL θ i as quantified by an increase in BrdU foci (Figures 1C and 1D). The BrdU foci overlapped with chromatin-bound RPA32, another marker of ssDNA, supporting the specificity of the staining (Figure 1C). Cells with increased numbers of BrdU foci displayed an increased nuclear size, potentially suggesting an effect of increased ssDNA gap formation on cell-cycle progression (Figures S1H and S1I).

To understand whether POL θ i-induced ssDNA is generated at replication forks, we used a modified DNA fiber assay, which includes S1 nuclease treatment. Cells were labeled with the

Figure 1. POL θ processes ssDNA gaps generated in BRCA1-deficient cells

(A) Computational docking model of small-molecule POL θ inhibitor (POL θ i) bound to the POL θ polymerase domain (PDB: 4X0P) with a detailed view of the allosteric binding pocket in the thumb region. Residues in proximity of the ligand (below 4A) are shown in gray. Two polar contacts with Gly2122 and Arg2201 are indicated in orange lines. Visualized with PyMOL (<http://www.pymol.org/pymol>).

(B) Clonogenic survival assays for RPE1 *TP53*^{-/-} and RPE1 *BRCA1*^{-/-} *TP53*^{-/-} cells treated with increasing concentrations of POL θ i with medium being replaced every 3 days. Representative images are shown in Figure S1D. Data represent mean \pm SD of n = 3.

(C) Representative images of SUM149PT treated with DMSO or 5 μ M POL θ i for 24 h and stained for RPA32 and BrdU under native conditions. Nuclear DNA was counterstained with DAPI. Scale bar: 5 μ m.

(D) Quantification of BrdU foci number per cell treated as indicated in (C). Only cells with ≥ 3 foci were quantified. At least 100 BrdU-positive cells were collected from n = 2. The median is indicated. p values were calculated using unpaired t test.

(E) Top: scheme of the CldU/IdU pulse-labeling protocol, followed by S1 nuclease treatment. Bottom: representative images of DNA fibers of RPE1 *TP53*^{-/-} and RPE1 *BRCA1*^{-/-} *TP53*^{-/-}, exposed to DMSO or 5 μ M POL θ i, with or without S1 nuclease treatment.

(F) IdU track lengths in RPE1 *TP53*^{-/-} cells with DMSO or POL θ i, with and without S1 nuclease treatment. p values were calculated using the Mann-Whitney test. Data represent mean \pm SD.

(G) Same as in (F) for RPE1 *BRCA1*^{-/-} *TP53*^{-/-}. p values were calculated using the Mann-Whitney test. Data represent mean \pm SD.

(H) Top: scheme of the CldU/IdU pulse-labeling protocol for DNA fiber assay. Bottom: representative images of CldU- and IdU-stained DNA fibers of RPE1 *TP53*^{-/-} and RPE1 *BRCA1*^{-/-} *TP53*^{-/-} with or without 5 μ M POL θ i.

(I) Fork speed of RPE1 *TP53*^{-/-} and RPE1 *BRCA1*^{-/-} *TP53*^{-/-} cells with and without POL θ i. At least 200 fibers were measured from n = 2. Data represent mean \pm SD. p values were calculated using the Mann-Whitney test.

(J) Fork arrest in RPE1 *TP53*^{-/-} and RPE1 *BRCA1*^{-/-} *TP53*^{-/-} cells treated with DMSO or POL θ i. High values indicate high symmetry, thus low levels of fork arrest. At least 200 fibers were measured from n = 2. Data represent mean \pm SD. p values were calculated using the Mann-Whitney test.

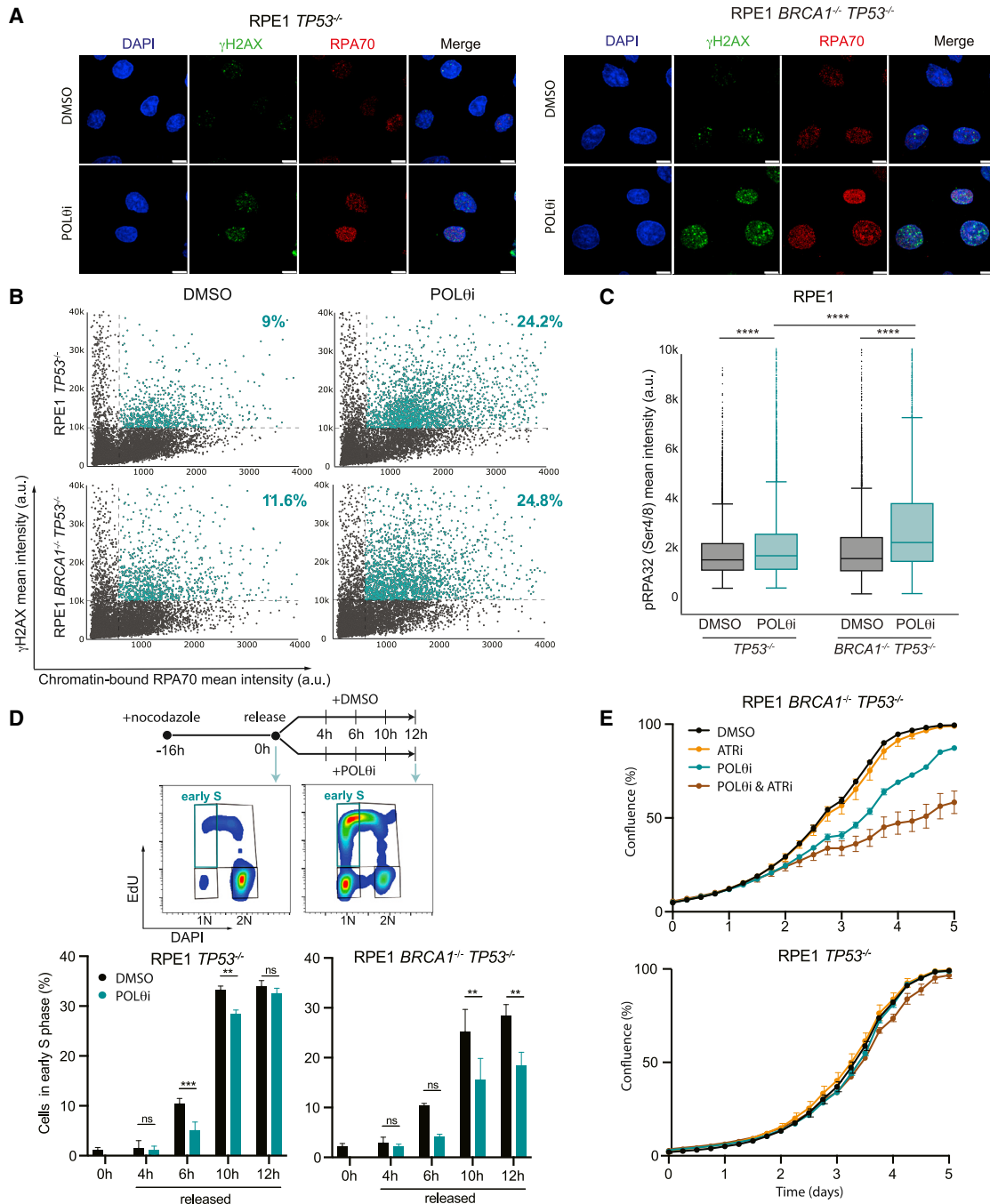


Figure 2. POL θ inhibition-induced replication stress is exacerbated in BRCA1-deficient cells

(A) Representative images of RPE1 *TP53*^{-/-} and RPE1 *BRCA1*^{-/-} *TP53*^{-/-} cells, treated with DMSO or 5 μ M POL θ i for 24 h, and stained for chromatin-bound RPA70 and γ H2AX. Nuclear DNA was counterstained with DAPI. 192 \times magnification. Scale bar: 10 μ m. See also Figure S2C.

(B) Quantification of mean intensity of chromatin-bound RPA32 and γ H2AX in RPE1 *TP53*^{-/-} and RPE1 *BRCA1*^{-/-} *TP53*^{-/-} cells treated as indicated in (A). Cells with a mean intensity higher than 800 a.u. for RPA70 and 10,000 a.u. for γ H2AX are marked in cyan and calculated for percentages. Each dot represents 1 cell. 8,800 cells were collected from $n = 2$. a.u., arbitrary units.

(C) Quantification of mean intensity of phosphorylated RPA32 (pRPA) at serine 4/8 in RPE1 *TP53*^{-/-} and RPE1 *BRCA1*^{-/-} *TP53*^{-/-} treated for 48 h with DMSO or 5 μ M POL θ i. At least 3,400 cells were collected from $n = 2$. p values were calculated with Kruskal-Wallis test. a.u., arbitrary units.

(D) Top: scheme of experimental setup and flow cytometry gating strategy. Cells were synchronized in G1 using a 16-h nocodazole treatment, followed by release in medium with DMSO or 5 μ M POL θ i and harvested at different time points after a 30-min EdU chase. (Bottom) Percentage of early S-phase cells at different time

(legend continued on next page)

nucleoside analogs CldU and IdU followed by incubation with S1 nuclease to digest regions of ssDNA²² (Figure 1E). Under vehicle treatment, S1 nuclease incubation did not affect the length of labeled tracks in RPE1 *TP53*^{-/-} cells, whereas RPE1 *BRCA1*^{-/-} *TP53*^{-/-} cells displayed shortened tracks, supporting an increased ssDNA burden in untreated BRCA1-deficient cells (Figures 1E–1G). POLθ inhibition led to a further decrease in track length specifically in BRCA1-deficient cells, indicating increased formation of replication gaps upon loss of POLθ (Figure 1G). These results suggest that ssDNA gaps are processed by POLθ in the absence of BRCA1.

To address the consequences of unfilled ssDNA gaps on replication fork progression, we assessed fork dynamics under POLθ inhibition. Independently of BRCA1 status, inhibition of POLθ resulted in decreased fork speed, as previously described¹³ (Figures 1H and 1I). Moreover, POLθ inhibition induced a significant decrease in the symmetry of IdU- and CldU-labeled tracks, specifically in BRCA1-deficient cells, indicating fork stalling (Figure 1J). Taken together, our findings reveal an undescribed function of POLθ in replication gap filling, which facilitates unperturbed replication fork progression in BRCA1-deficient cells.

POLθ inhibition-induced replication stress is exacerbated in BRCA1-deficient cells

We next sought to identify the cellular consequences of impaired replication fork progression in the absence of POLθ. After treatment with replication stress-inducing agents, RPA has been shown to coat regions of ssDNA to protect it from nucleolytic attack. When RPA levels become limiting, unprotected ssDNA is converted to DSBs, which are signaled by γH2AX.¹¹ To determine if cells lacking POLθ activity exhibit elevated levels of replication stress, we quantified γH2AX as well as chromatin-bound RPA70 in RPE1 *TP53*^{-/-}, RPE1 *BRCA1*^{-/-} *TP53*^{-/-}, and SUM149PT cells. POLθ inhibition increased the percentage of cells positive for markers of ssDNA and DSBs (Figures 2A, 2B, and S2A–S2C), suggesting that the compromised replication fork integrity in the absence of POLθ affects overall replication stress levels. Given the specific sensitivity of BRCA1-deficient cells to POLθ inhibition, we asked whether the observed replication stress is less tolerated in the absence of BRCA1. Indeed, RPE1 *BRCA1*^{-/-} *TP53*^{-/-} showed increased phosphorylation of RPA32 at serine 4/8, a known replication stress signal, at later time points after POLθ inhibition, indicating that replication stress induced by POLθ inhibition is poorly resolved in BRCA1-deficient cells (Figures 2C and S2D).

We next determined whether increased ssDNA gaps and replication stress impact cell-cycle progression of cells lacking POLθ activity. Thus, we synchronized RPE1 cells in the G2/M phase of the cell cycle using nocodazole, followed by release into medium containing DMSO or POLθi. At early time points after release, POLθ inhibition induced a delay of S-phase entry in both cell lines. However, while the cell-cycle profile of POLθi- and DMSO-

treated RPE1 *TP53*^{-/-} is indistinguishable at 12 h after release, POLθ inhibition causes a consistent delay of S-phase entry in BRCA1-deficient cells also at later time points (Figure 2D).

Considering the elevated levels of ssDNA and replication stress in BRCA1-deficient cells under POLθ inhibition, we determined whether POLθi treatment would synergize with replication-stress-inducing agents. Given that the kinase ATR functions to suppress replication stress by reducing origin firing, thereby limiting the formation of ssDNA, we tested POLθ inhibition in combination with the ATR inhibitor ceralasertib. Indeed, a sublethal dose of ceralasertib specifically sensitized RPE1 *BRCA1*^{-/-} *TP53*^{-/-} to POLθi (Figure 2E). Co-treatment with the translesion synthesis inhibitor JH-RE-06²³ showed an additive drug effect in BRCA1-deficient RPE1 cells, suggesting that POLθ and translesion polymerases might have non-overlapping functions in gap filling (Figure S2E). The above data suggest that a lack of POLθ activity leads to replication stress, causing prolonged replication stress signaling and defects in cell-cycle progression in BRCA1-deficient cells, which can be exacerbated with ATR inhibitor co-treatment.

A genome-wide CRISPR-Cas9 KO screen identified modulators of the BRCA1-POLθ interaction

POLθ is an emerging drug target in BRCA1/2-deficient cancers.¹⁷ Therefore, understanding the cellular factors that impact this genetic interaction might inform on clinically relevant drug modulators. To this end, we performed a genome-wide CRISPR-Cas9 KO screen in a cellular model of breast cancer, a cancer type that is included in ongoing clinical trials with POLθis (A Study of ART4215 for the Treatment of Advanced or Metastatic Solid Tumors, [ClinicalTrials.gov](https://clinicaltrials.gov/ct2/show/study/NCT04991480): NCT04991480). We transduced SUM149PT cells with a lentiviral pool encoding the genome-wide Toronto v.3 guide RNA (gRNA) library (TKOv.3)²⁴ and selected transduced cells with puromycin. To enrich for suppressors of drug response, transduced cells were exposed to 2–2.5 μM of POLθi, a dose determined to kill 90% of the cell population (LD₉₀), or DMSO for 18 days (Figures S3A and S3B). Next, we extracted genomic DNA with integrated gRNA sequences and used next-generation sequencing (NGS) to identify gRNA abundances (Figure 3A). For quality control, we compared gRNA abundance between end (day 18 of treatment) and early time point samples, which were collected 5 days after puromycin selection. gRNAs targeting essential genes were depleted in the late time point of both DMSO- and POLθi-treated screens, whereas control gRNAs such as those targeting olfactory receptor genes had no effect on cellular survival (Figures S3C and S3D). To identify sensitizers of POLθi, we focused on gRNAs that are depleted in POLθi-treated, compared with DMSO-treated, samples. As expected, gRNAs targeting HR pathway factors, such as RAD51C, were among the top depleted hits (Figure S3E). Moreover, gRNAs targeting several factors of the Fanconi anemia pathway, which is involved in replication fork stabilization beyond its role in inter-strand crosslink repair, were also depleted (Figure S3E).

points after release from nocodazole synchronization in DMSO or 5 μM POLθi containing medium. Data represent mean ± SD. At least 10,000 singlets were collected from n = 2. p values were calculated with unpaired t test.

(E) Confluence of RPE1 *TP53*^{-/-} and RPE1 *BRCA1*^{-/-} *TP53*^{-/-} over 5 days of single or dual ATRi (500 nM)/POLθi (3 μM) treatment, detected by Incucyte live-cell imaging. The data represent mean ± SD of two technical replicates.

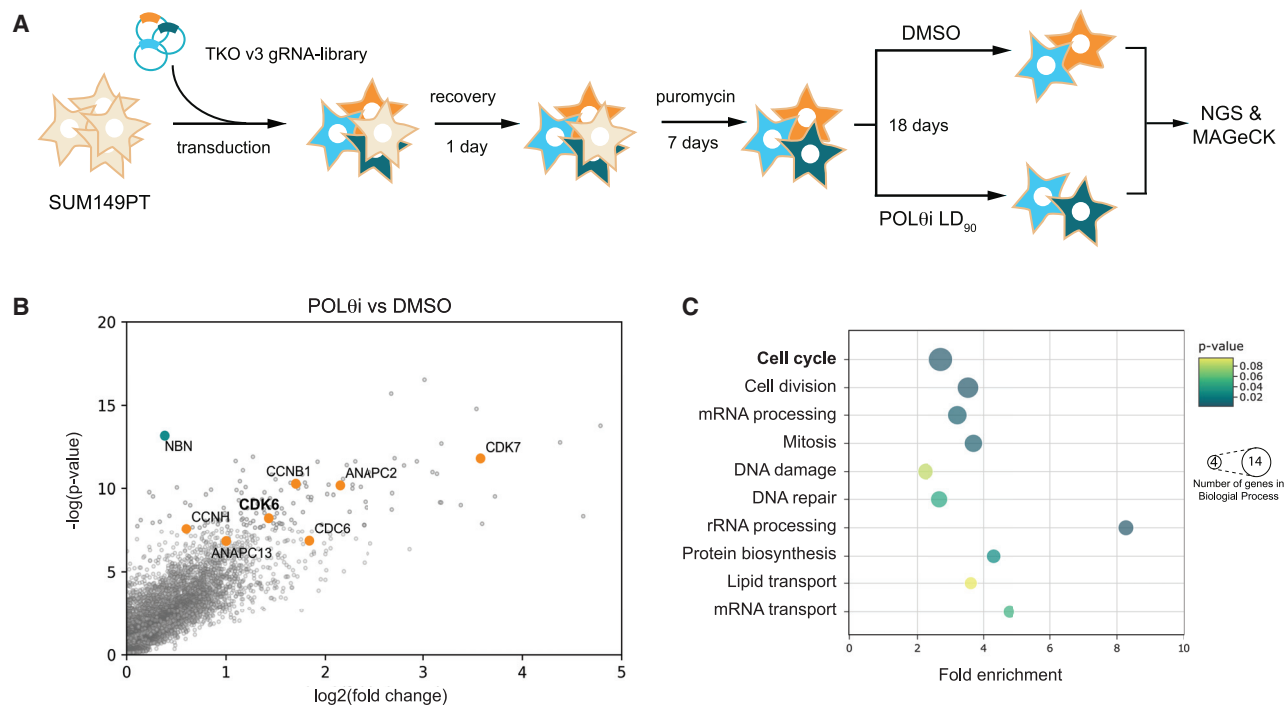


Figure 3. A genome-wide CRISPR-Cas9 KO screen identified modulators of the BRCA1-POLθ genetic interaction

(A) Scheme of the experimental setup of the genome-wide CRISPR-Cas9 KO screen. SUM149PT cells were transduced with the TKOv.3 gRNA library, and puromycin was added after 1 day of recovery. After 7 days of antibiotic selection, cells were either treated with DMSO or 2–2.5 μ M POLθi over 18 days, followed by genomic DNA extraction and NGS for determining gRNA abundances.

(B) Scatterplot of MAGeCK analysis of genome-wide CRISPR-Cas9 KO screen in POLθi-treated SUM149PT normalized to DMSO. Only genes with $\log_2(\text{fold change}) > 0$ are shown. Cell-cycle genes as well as genes of the MRN complex are highlighted in orange and cyan, respectively.

(C) Top 10 GO terms of genes targeted by enriched gRNAs ($p < 0.005$), identified using DAVID Bioinformatics Resources.^{25,26}

To determine genes that facilitate the functional interaction between POLθ and BRCA1, we focused on enriched gRNAs (Figure 3B). This led to the identification of NBN, a component of the MRN complex reported to function in replication fork stability.² Interestingly, we saw an enrichment of cell-cycle regulators, including CDK6, a target that is currently exploited in breast cancer therapy, through the use of CDK4/6 inhibitors.²⁷ To annotate the top enriched biological processes among significant positive hits ($p < 0.005$), we used the DAVID GO-term analysis tool,^{25,26} identifying the terms “cell cycle” and “cell division” as top enriched terms (Figure 3C). In summary, an unbiased genome-wide CRISPR-Cas9 KO screen identified the MRN complex and cell-cycle regulators as modulators of the genetic interaction between BRCA1 and POLθ.

Loss of activity of the MRN complex and CDK6 alleviates the functional interaction between BRCA1 and POLθ

To investigate the molecular mechanism by which loss of MRN complex activity suppresses the functional interaction between BRCA1 and POLθ, we compared the levels of chromatin-bound RPA upon single or combined inhibition of POLθ and MRE11. As described above, POLθ inhibition increased RPA chromatin binding and γ H2AX levels in RPE1 *BRCA1*^{-/-} *TP53*^{-/-}. However, concomitant treatment with mirin, a small-molecule inhibitor of MRE11 activity, suppressed RPA chromatin binding and

decreased H2AX phosphorylation compared with POLθ inhibition alone²⁸ (Figure 4A). These data suggest that the MRN complex cleaves and processes ssDNA that accumulates in BRCA1-deficient cells lacking POLθ activity, thus promoting ssDNA accumulation, formation of DNA DSBs, and cell death. Thus, the MRN complex partially drives the toxicity of the functional interaction between BRCA1 and POLθ in the cellular replication stress response.

To further understand how loss of CDK6 activity alleviates the hypersensitivity of BRCA1-deficient cells to POLθ inhibition, we took advantage of the selective CDK4/6 inhibitor palbociclib.²⁷ As expected, CDK4/6 inhibition efficiently increased the percentage of cells in the G1 phase of the cell cycle by delaying S-phase entry (Figures 4B and S4A). To address the effect of reduced S-phase entry on replication stress levels, we stained for chromatin-bound RPA32 and γ H2AX. Compared with POLθi treatment alone, CDK4/6i co-treatment drastically alleviated replication stress, as shown by decreased RPA chromatin binding and nuclear γ H2AX signal (Figures 4C, S4B, and S4C). To further explore the genetic interaction between CDK6 and POLθ without affecting CDK4 activity, we generated stable KO cell lines of CDK6 in SUM149PT. To clarify whether the alleviated replication stress with loss of CDK6 activity also translates into increased viability, we compared proliferation of CDK6 KO and control SUM149PT in the presence of POLθi by Incucyte

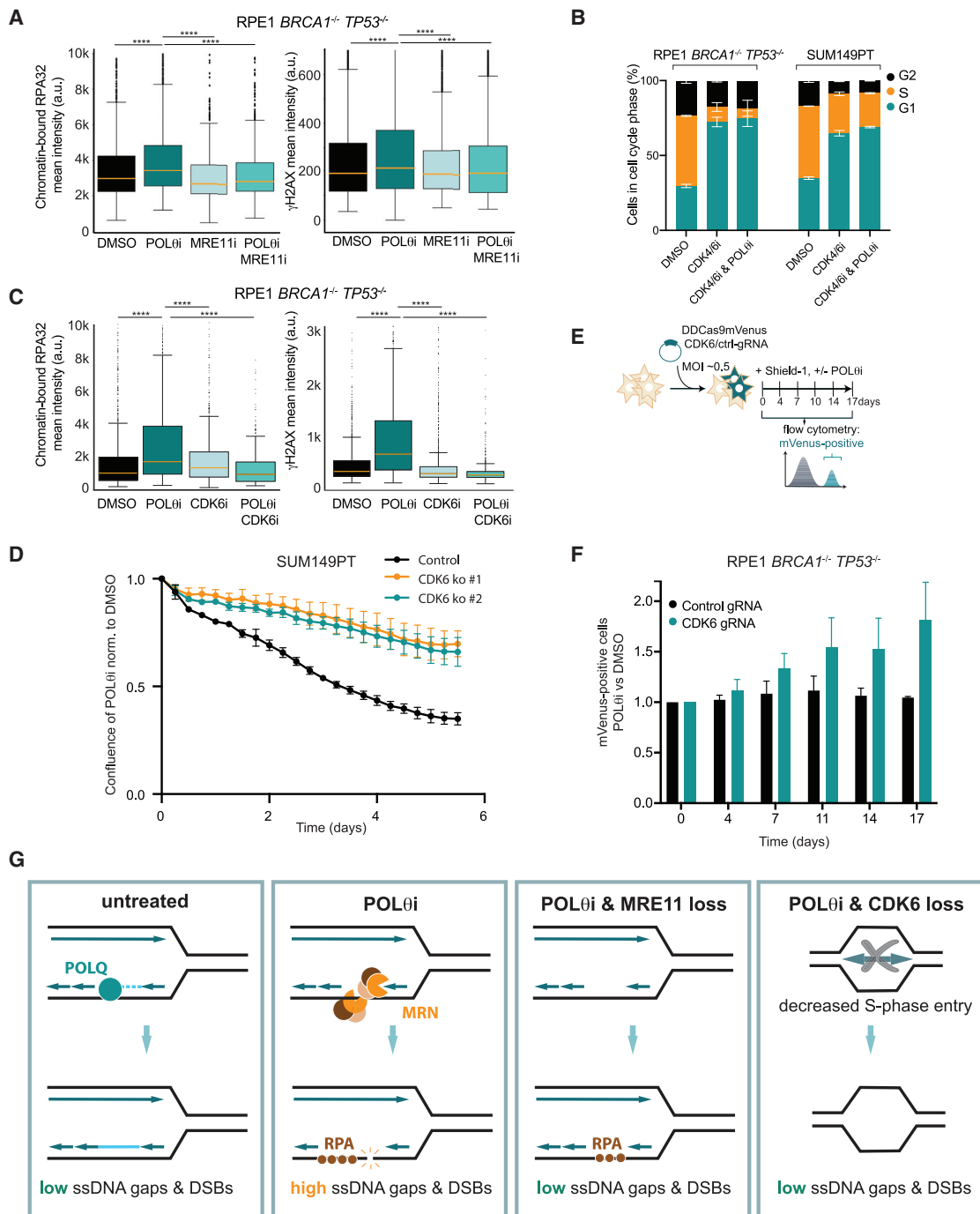


Figure 4. Loss of activity of the MRN complex and CDK6 alleviate the functional interaction between BRCA1 and POLQ

(A) Quantification of immunofluorescence showing chromatin-bound RPA32 and γ H2AX mean intensity levels in RPE1 *BRCA1*^{-/-} *TP53*^{-/-} cells treated for 6 h with DMSO, 5 μ M POL θ i, and/or 50 μ M MRE11i. At least 5,000 cells were collected from $n = 2$. a.u., arbitrary units.

(B) RPE1 *BRCA1*^{-/-} *TP53*^{-/-} and SUM149PT were treated for 24 (RPE1) or 48 h (SUM149PT) with DMSO, 5 μ M POL θ i, and/or 1 μ M CDK4/6i followed by a 30 min EdU chase to label newly synthesized DNA. Data represent mean \pm SD. At least 20,000 singlets were collected from $n = 2$. Representative flow cytometry plots and gating strategy are shown in Figure S4A.

(C) Quantification of immunofluorescence showing chromatin-bound RPA32 and γ H2AX mean intensity levels in RPE1 *BRCA1*^{-/-} *TP53*^{-/-} cells after 24 h of single or dual POL θ i (5 μ M)/CDK4/6i(1 μ M) treatment. At least 500 cells were collected from $n = 2$.

(D) Confluence of SUM149PT transduced with control or one of two independent CDK6-gRNAs with 5 μ M POL θ i treatment normalized to DMSO, detected by Incucyte live-cell imaging. The corresponding proliferation curves for both DMSO and POL θ i are shown in Figure S4D. Data represent mean \pm SD of 3 technical replicates and are a representative set of images of $n = 2$.

(legend continued on next page)

live-cell imaging. Indeed, CDK6 loss, induced by two independent gRNAs, increased proliferation of SUM149PT under POL θ inhibition compared with cells transduced with a control gRNA (Figures 4D and S4D). This rescue was also observed in BRCA1-deficient RPE1 during long-term POL θ i treatments with replenished fresh compound every 3 days while not influencing the POL θ i response of BRCA1 wild-type RPE1 cells (Figure S4E). To assess the kinetics of CDK6-dependent alleviation of POL θ i response, we utilized an inducible Cas9 expression system to target CDK6 and monitored growth of control and BRCA1-deficient RPE cells under POL θ i or DMSO treatment in a competitive growth assay (Figure 4E).²⁹ Whereas CDK6 loss had only a minor effect on POL θ i response of RPE1 *TP53*^{-/-} (Figure S4F), it alleviated the toxicity of POL θ i in RPE1 *BRCA1*^{-/-} *TP53*^{-/-}, starting from 4 days after treatment (Figure 4F). Overall, we have shown that the genetic interaction between BRCA1 and POL θ depends on ssDNA, a substrate for nucleolytic processing by the MRN complex, which is specifically formed in dividing cells, explaining why CDK6 loss provides a fitness advantage in response to POL θ inhibition.

DISCUSSION

The occurrence of replication gaps across the genome has challenged the hypothesis that DSBs are the main drivers of cellular toxicity upon treatment with PARP inhibitors or genotoxic agents such as cisplatin.^{7,10} In this study, we propose that ssDNA gap formation contributes to the synthetic lethality between BRCA1 and POL θ . Using a small-molecule inhibitor targeting the POL θ polymerase domain, we directly visualized gaps by immunofluorescence and DNA fiber assays. Previous work has demonstrated an increase in BrdU foci in mouse embryonic fibroblasts lacking both BRCA1 and the end protection factor 53BP1 using another small-molecular inhibitor of POL θ .¹⁸ The elevated BrdU foci number was attributed to increased resection at DNA DSBs. Using S1 nuclease fiber assays, we show that POL θ inhibition in BRCA1-deficient cells results in elevated levels of ssDNA that arise, at least partially, from replication gaps. Given that the inhibitor used in this study targets the POL θ polymerase domain, we hypothesize that POL θ exerts its function in gap filling through utilizing its translesion synthesis activity.³⁰ In line with our study, loss of gap filling by inhibition of other translesion synthesis polymerases, for example by the REV1-Pol ζ inhibitor JH-RE-06, has been shown to expose ssDNA gaps as a cancer vulnerability.^{5,31} Moreover, inhibitors of translesion synthesis have been shown to synergize with other gap-inducing treatments such as ATR inhibition.³¹ This is consistent with our finding that ATR inhibition synergizes with POL θ inhibition in BRCA1-deficient cells. However, it remains poorly understood why other translesion synthesis (TLS) polymerases cannot fully

compensate for POL θ loss in BRCA1-deficient cells. Potentially, POL θ is preferred over other TLS polymerases because it contains not only a polymerase domain capable of filling ssDNA gaps but also a helicase domain that could process flap structures that are generated during the removal of the DNA-RNA primers of downstream Okazaki fragments.²¹

Previously, PARP1 was shown to recruit POL θ to sites of DNA DSBs.¹⁴ Since PARP1 functions as a sensor of unligated Okazaki fragments on the lagging strand,⁹ we speculate that PARP1 might recruit POL θ to sites of ssDNA gaps. An alternative, not mutually exclusive, mode of recruitment could be through TLS signaling, as POL θ has been shown to bind ubiquitinated PCNA in UV-irradiated human fibroblasts.¹⁶ Moreover, POL θ is known to displace RAD51 from ssDNA overhangs of resected DSBs, thereby determining the DSB pathway choice between HR and TMEJ.¹³ We hypothesize that this displacement might also function in the context of ssDNA gaps that are recognized by RAD51. Furthermore, the POL θ helicase domain was shown to preferentially unwind lagging strands of substrates resembling stalled replication forks.³² We hypothesize that DNA unwinding by POL θ may allow access to ssDNA gaps formed on the lagging strand for subsequent gap filling. Taken together, we propose a hypothetical model in which POL θ is recruited by PARP1 or TLS signaling to function in ssDNA gap filling by combining helicase-dependent unwinding of the lagging strand, RAD51 displacement, and TLS activity.

Here, we show that lack of ssDNA processing by POL θ alters replication fork dynamics in BRCA1-deficient cells, leading to asymmetric fork progression and consecutive replication stress. Previous studies have implicated POL θ in the response to replication stress induced by hydroxyurea as well as in the regulation of replication timing under unchallenged conditions.³³⁻³⁵ We reason that the endogenous functions of POL θ in replication progression become apparent in genetic backgrounds with increased steady-state replication stress, such as BRCA1 deficiency. Furthermore, POL θ has been shown to bind to the origin recognition complex, bringing it in close physical proximity with replication forks, the sites of potential ssDNA formation.³⁴ Altogether, these findings suggest that tight regulation of POL θ activity with respect to replication is essential, both in wild-type cells to ensure genome integrity and in BRCA1-deficient cells where POL θ becomes essential for cell survival.

We identified NBN, a member of the MRN complex, as a suppressor of the genetic interaction between BRCA1 and POL θ . Given the known role of BRCA1/2 in limiting MRN complex activity, we hypothesize that the MRN complex destabilizes the genome by processing replication gaps, which are formed in the context of POL θ inhibition, into DSBs^{2,36} (Figure 4G). In support of this, we show that short-term inhibition of MRE11 activity alleviates replication stress in response to POL θ inhibition.²¹

(E) Experimental setup of competitive growth assay. RPE1 *TP53*^{-/-} and RPE1 *BRCA1*^{-/-} *TP53*^{-/-} cells were transduced with control or CDK6 gRNAs at an approximate multiplicity of infection (MOI) of 0.5 and seeded with Shield-1 to induce Cas9 expression in the presence or absence of POL θ i 2 days later. Flow cytometry was used to measure the growth kinetics of KO (i.e., mVenus-positive) cells over time.

(F) mVenus-positive RPE1 *BRCA1*^{-/-} *TP53*^{-/-} cells under POL θ i treatment normalized to DMSO over time, treated as indicated in (E). Data represent mean \pm SD of 2 biological replicates. For RPE1 *TP53*^{-/-} cells, see Figure S4F.

(G) Proposed model explaining modulatory effects of the MRN complex and CDK6 on the BRCA1-POL θ genetic interaction, as shown based on a replication fork in a BRCA1-deficient cell.

Future studies will be necessary to address the downstream processing of ssDNA gaps in the absence of MRE11 and POL θ activity. Further to this, we identified an enrichment of cell-cycle regulators as modulators of POL θ i response in BRCA1-deficient cells. We show that CDK6 activity facilitates cell-cycle progression, thus exacerbating POL θ i-induced replication stress (Figure 4G). This can be suppressed by genetic loss of CDK6 or by inhibiting CDK4/6 activity with the small molecule palbociclib, which has been FDA approved for the treatment of specific subtypes of breast cancer.²⁷ Our results suggest that concomitant application of CDK6 and POL θ is might have antagonistic effects, an important insight when considering the future clinical use of POL θ is.

In conclusion, we leveraged single-molecule approaches as well as high-throughput genomics to dissect the genetic interaction between POL θ and BRCA1, thus identifying their converging roles in maintaining replication fork stability as fundamental to their synthetic lethal relationship. Furthermore, the role of POL θ in ssDNA processing is conserved in BRCA2-deficient cells, strengthening the importance of POL θ function for genome stability in BRCA mutant cells.²¹ Our findings provide important insights into POL θ and BRCA1 biology that are especially valuable given that clinical trials with POL θ is are ongoing.

Limitations of the study

Here, we report an increase in ssDNA gaps upon POL θ inhibition in a BRCA1-deficient background. However, we cannot comment on size and location of these gaps. Electron microscopy, which could provide more detailed insights into gap kinetics and position, is technically challenging to perform due to the extreme sensitivity of BRCA1-defective cells to POL θ inhibition, preventing the collection of sufficient amounts of intact genomic DNA. Another potential limitation of this study is the lack of a genetic model for POL θ loss. Since BRCA1 and POL θ share a lethal interaction, the generation of cell lines that are genetically deficient for both factors is challenging. Therefore, future studies using different POL θ is, potentially also targeting different enzymatic domains, will be necessary to fully characterize the underlying molecular mechanisms.

STAR★METHODS

Detailed methods are provided in the online version of this paper and include the following:

- KEY RESOURCES TABLE
- RESOURCE AVAILABILITY
 - Lead contact
 - Materials availability
 - Data and code availability
- EXPERIMENTAL MODEL AND SUBJECT DETAILS
 - Cell lines and culture conditions
- METHOD DETAILS
 - Plasmids
 - Competitive growth assay
 - Generation of cell lines
 - Cell growth assays
 - Genome-wide CRISPR-Cas9 ko screen

- Immunoblotting
- Compounds and inhibitors
- Flow cytometry
- Cell cycle synchronization
- Gene ontology-term analysis
- Identification and scoring of a POL θ i binding pocket in the POL θ polymerase domain
- DNA fiber assay
- S1 nuclease assay
- Immunofluorescence and imaging
- QUANTIFICATION AND STATISTICAL ANALYSIS
 - Statistical analysis

SUPPLEMENTAL INFORMATION

Supplemental information can be found online at <https://doi.org/10.1016/j.celrep.2022.111716>.

ACKNOWLEDGMENTS

We would like to thank the VBCF (Vienna, Austria) for next-generation sequencing. We would like to acknowledge Jacob Corn (ETHZ, Zurich, Switzerland), Stephen Jackson (The Gurdon Institute, Cambridge, UK), and their teams as well as members of the Loizou laboratory for helpful discussions and feedback. We would like to thank Yaron Galanty and Rimma Belotserkovskaya (The Gurdon Institute, Cambridge, UK) as well as Sabbi Lall (Life Science Editors) for critical reading of the manuscript. We also thank the laboratory of Stephen Jackson for sharing RPE1 *TP53*^{-/-} and SUM149PT cell lines and the laboratory of Daniel Durocher (Lunenfeld-Tanenbaum Research Institute, Toronto, ON, Canada) for sharing RPE1 *BRCA1*^{-/-} *TP53*^{-/-} cell lines. A.S. is supported by a DOC fellowship from the Austrian Academy of Sciences (25524). S.B. is funded by the Austrian Science Fund (F79 Spezialforschungsbereiche). The Loizou lab is funded by an ERC Synergy Grant (DDREAMM grant agreement ID: 855741, awarded to J.I.L.). CeMM is funded by the Austrian Academy of Sciences. The work of V.C. has been supported by Associazione Italiana per la Ricerca sul Cancro, AIRC-IG ref. 21824, and by an AIRC-FIRC fellowship assigned to M.A.R.O. (ref. 2531).

AUTHOR CONTRIBUTIONS

A.S., S.B., and J.I.L. conceptualized the study. A.S., S.B., E.A.A.V., M.A.R.O., and J.W. curated data. D.K. and G.T. contributed to microscopy. A.M.A., A.K., and M.W. performed the *in silico* docking analysis. A.S. and S.B. performed analysis and visualization. G.F.E., V.C., G.E.W., and J.I.L. supervised and carried out project administration associated with the study. A.S. and S.B., with input from J.I.L., wrote the original draft, and all authors reviewed and edited the final manuscript. A.S. and J.I.L. obtained funding.

DECLARATION OF INTERESTS

J.I.L. is now an employee of AstraZeneca.

Received: March 18, 2022

Revised: August 21, 2022

Accepted: November 2, 2022

Published: November 17, 2022

REFERENCES

1. Apostolou, P., and Fostira, F. (2013). Hereditary breast cancer: the Era of new susceptibility genes. *BioMed Res. Int.* <https://doi.org/10.1155/2013/747318>.
2. Hashimoto, Y., Chaudhuri, A.R., Lopes, M., and Costanzo, V. (2010). Rad51 protects nascent DNA from Mre11-dependent degradation and

- promotes continuous DNA synthesis. *Nat. Struct. Mol. Biol.* 17, 1305–1311. <https://doi.org/10.1038/nsmb.1927>.
3. Chaudhuri, A.R., Callen, E., Ding, X., Gogola, E., Duarte, A.A., Lee, J.E., Wong, N., Lafarga, V., Calvo, J.A., Panzarino, N.J., et al. (2016). Replication fork stability confers chemoresistance in BRCA-deficient cells. *Nature* 535, 382–387. <https://doi.org/10.1038/nature18325>.
 4. Kolinjivadi, A.M., Sannino, V., De Antoni, A., Zadorozhny, K., Kilkenny, M., Técher, H., Baldi, G., Shen, R., Ciccio, A., Pellegrini, L., et al. (2017). Smc1-Mediated fork reversal triggers mre11-dependent degradation of nascent DNA in the absence of Brca2 and stable Rad51 nucleofilaments. *Mol. Cell* 67, 867–881.e7. <https://doi.org/10.1016/j.molcel.2017.07.001>.
 5. Tagliatalata, A., Leuzzi, G., Sannino, V., Cuella-Martin, R., Huang, J.-W., Wu-Baer, F., Baer, R., Costanzo, V., and Ciccio, A. (2021). REV1-Pol ζ maintains the viability of homologous recombination-deficient cancer cells through mutagenic repair of PRIMPOL-dependent ssDNA gaps. *Mol. Cell* 1–18. <https://doi.org/10.1016/j.molcel.2021.08.016>.
 6. Tagliatalata, A., Alvarez, S., Leuzzi, G., Sannino, V., Ranjha, L., Huang, J.W., Madubata, C., Anand, R., Levy, B., Rabadan, R., et al. (2017). Restoration of replication fork stability in BRCA1- and BRCA2-deficient cells by inactivation of SNF2-family fork remodelers. *Mol. Cell* 68, 414–430.e8. <https://doi.org/10.1016/j.molcel.2017.09.036>.
 7. Cong, K., Peng, M., Kousholt, A.N., Lee, W.T.C., Lee, S., Nayak, S., Kraiss, J., VanderVere-Carozza, P.S., Pawelczak, K.S., Calvo, J., et al. (2021). Replication gaps are a key determinant of PARP inhibitor synthetic lethality with BRCA deficiency. *Mol. Cell* 81, 3128–3144.e7. <https://doi.org/10.1016/j.molcel.2021.06.011>.
 8. Dias, M.P., Tripathi, V., Heijden, I.V.D., Cong, K., Bhin, J., Gogola, E., Galanos, P., Annunziato, S., Chakrabarty, S., Smith, G.C.M., et al. (2021). Loss of nuclear DNA ligase III reverts PARP inhibitor resistance in BRCA1/53BP1 double-deficient cells by exposing ssDNA gaps. *Mol. Cell* 1–17. <https://doi.org/10.1016/j.molcel.2021.09.005>.
 9. Hanzlikova, H., Kalasova, I., Demin, A.A., Pennicott, L.E., Cihlarova, Z., and Caldecott, K.W. (2018). The importance of poly(ADP-ribose) polymerase as a sensor of unligated Okazaki fragments during DNA replication. *Mol. Cell* 71, 319–331.e3. <https://doi.org/10.1016/j.molcel.2018.06.004>.
 10. Panzarino, N.J., Kraiss, J.J., Cong, K., Peng, M., Mosqueda, M., Nayak, S.U., Bond, S.M., Calvo, J.A., Doshi, M.B., Bere, M., et al. (2021). Replication gaps underlie BRCA deficiency and therapy response. *Cancer Res.* 81, 1388–1397. <https://doi.org/10.1158/0008-5472.CAN-20-1602>.
 11. Toledo, L.I., Altmeyer, M., Rask, M.B., Lukas, C., Larsen, D.H., Povlsen, L.K., Bekker-Jensen, S., Mailand, N., Bartek, J., and Lukas, J. (2013). ATR prohibits replication catastrophe by preventing global exhaustion of RPA. *Cell* 155, 1088. <https://doi.org/10.1016/j.cell.2013.10.043>.
 12. Lord, C.J., and Ashworth, A. (2013). Mechanisms of resistance to therapies targeting BRCA-mutant cancers. *Nat. Med.* 19, 1381–1388. <https://doi.org/10.1038/nm.3369>.
 13. Ceccaldi, R., Liu, J.C., Amunugama, R., Hajdu, I., Primack, B., Petalcorin, M.I.R., O'Connor, K.W., Konstantinopoulos, P.A., Elledge, S.J., Boulton, S.J., et al. (2015). Homologous-recombination-deficient tumours are dependent on Pol θ -mediated repair. *Nature* 518, 258–262. <https://doi.org/10.1038/nature14184>.
 14. Mateos-Gomez, P.A., Gong, F., Nair, N., Miller, K.M., Lazzarini-Denchi, E., and Sfeir, A. (2015). Mammalian polymerase θ promotes alternative NHEJ and suppresses recombination. *Nature* 518, 254–257. <https://doi.org/10.1038/nature14157>.
 15. Koole, W., Van Schendel, R., Karambelas, A.E., Van Heteren, J.T., Okihara, K.L., and Tijsterman, M. (2014). A polymerase theta-dependent repair pathway suppresses extensive genomic instability at endogenous G4 DNA sites. *Nat. Commun.* 5, 1–10. <https://doi.org/10.1038/ncomms4216>.
 16. Yoon, J.H., McArthur, M.J., Park, J., Basu, D., Wakamiya, M., Prakash, L., and Prakash, S. (2019). Error-prone replication through UV lesions by DNA polymerase θ protects against skin cancers. *Cell* 176, 1295–1309.e15. <https://doi.org/10.1016/j.cell.2019.01.023>.
 17. Schrepf, A., Slyskova, J., and Loizou, J.I. (2021). Targeting the DNA repair enzyme polymerase θ in cancer therapy. *Trends in Cancer* 7, 98–111. <https://doi.org/10.1016/j.trecan.2020.09.007>.
 18. Zatreanu, D., Robinson, H.M.R., Alkhatib, O., Boursier, M., Finch, H., Geo, L., Grande, D., Grinkevich, V., Heald, R.A., Langdon, S., et al. (2021). Pol θ inhibitors elicit BRCA-gene synthetic lethality and target PARP inhibitor resistance. *Nat. Commun.* 1–15. <https://doi.org/10.1038/s41467-021-23463-8>.
 19. Zhou, J., Gelot, C., Pantelidou, C., Li, A., Yücel, H., Davis, R.E., Färkkilä, A., Kochupurakkal, B., Syed, A., Shapiro, G.I., et al. (2021). A first-in-class polymerase theta inhibitor selectively targets homologous-recombination deficient tumors. *Nat. Cancer.* <https://doi.org/10.1038/s43018-021-00203-x>.
 20. Blencowe, P., Charles, M., Cridland, A., Ekwuru, T., Heald, R., Macdonald, E., McCarron, H., and Rigoreau, L. (2020). Heterocyclic substituted ureas, for use against cancer. WO patent WO-2020030925-A1. Filed August 9, 2018, and published February 13, 2020.
 21. Mann, A., Ramirez-Otero, M.A., De Antoni, A., Hanthi, Y.W., Sannino, V., Baldi, G., Falbo, L., Schrepf, A., Bernardo, S., Loizou, J., et al. (2022). POL θ prevents MRE11-NBS1-CtIP-dependent fork breakage in the absence of BRCA2/RAD51 by filling lagging-strand gaps. *Mol Cell* 82, S1097-2765(22)00902-9. <https://doi.org/10.1016/j.molcel.2022.09.013>.
 22. Quinet, Annabel, Carvajal-Maldonado, Denisse, Lemacon, Delphine, and Vindigni, Alessandro (2017). DNA Fiber Analysis: Mind the Gap! *Methods in Enzymology* 591 (May), 55–82, In press. [#">https://doi.org/10.1016/bs.mie.2017.03.019 #](https://doi.org/10.1016/bs.mie.2017.03.019).
 23. Wojtaszek, J.L., Chatterjee, N., Najeeb, J., Ramos, A., Lee, M., Bian, K., Xue, J.Y., Fenton, B.A., Park, H., Li, D., et al. (2019). A small molecule targeting mutagenic translesion synthesis improves chemotherapy. *Cell* 178, 152–159.e11. <https://doi.org/10.1016/j.cell.2019.05.028>.
 24. Hart, T., Tong, A.H.Y., Chan, K., Van Leeuwen, J., Seetharaman, A., Aregger, M., Chandrashekar, M., Hustedt, N., Seth, S., Noonan, A., et al. (2017). Evaluation and design of genome-wide CRISPR/SpCas9 knockout screens. *G3 Genes, Genomes, Genet.* 7, 2719–2727. <https://doi.org/10.1534/g3.117.041277>.
 25. Huang, D.W., Sherman, B.T., and Lempicki, R.A. (2009a). Systematic and integrative analysis of large gene lists using DAVID bioinformatics resources. *Nat. Protoc.* 4, 44–57. <https://doi.org/10.1038/nprot.2008.211>.
 26. Huang, D.W., Sherman, B.T., and Lempicki, R.A. (2009b). Bioinformatics enrichment tools: paths toward the comprehensive functional analysis of large gene lists. *Nucleic Acids Res.* 37, 1–13. <https://doi.org/10.1093/nar/gkn923>.
 27. Fry, D.W., Harvey, P.J., Keller, P.R., Elliott, W.L., Meade, M., Trachet, E., Albassam, M., Zheng, X., Leopold, W.R., Pryer, N.K., et al. (2004). Specific inhibition of cyclin-dependent kinase 4/6 by PD 0332991 and associated antitumor activity in human tumor xenografts. *Mol. Cancer Ther.* 3, 1427–1438. <https://doi.org/10.1158/1535-7163.1427.3.11>.
 28. Dupré, A., Boyer-Chatenet, L., Sattler, R.M., Modi, A.P., Lee, J.H., Nicolette, M.L., Kopelovich, L., Jasin, M., Baer, R., Paull, T.T., et al. (2008). A forward chemical screen reveals an inhibitor of the Mre11-Rad50-Nbs1 complex. *Nat. Chem. Biol.* 4, 119–125. <https://doi.org/10.1038/nchembio.63>.
 29. Senturk, S., Shirole, N.H., Nowak, D.G., Corbo, V., Pal, D., Vaughan, A., Tuveson, D.A., Trotman, L.C., Kinney, J.B., and Sordella, R. (2017). Rapid and tunable method to temporally control gene editing based on conditional Cas9 stabilization. *Nat. Commun.* 8, 1–10. <https://doi.org/10.1038/ncomms14370>.
 30. Hogg, M., Seki, M., Wood, R.D., Doublé, S., and Wallace, S.S. (2011). Lesion bypass activity of DNA polymerase θ (POLQ) is an intrinsic property of the pol domain and depends on unique sequence inserts. *J. Mol. Biol.* 405, 642–652. <https://doi.org/10.1016/j.jmb.2010.10.041>.
 31. Nayak, S., Calvo, J.A., Cong, K., Peng, M., Berthiaume, E., Jackson, J., Zaino, A.M., Vindigni, A., Hadden, M.K., and Cantor, S.B. (2020). Inhibition of the translesion synthesis polymerase REV1 exploits replication gaps as

- a cancer vulnerability. *Sci. Adv.* **6**. <https://doi.org/10.1126/sciadv.aaz7808>.
32. Ozdemir, A.Y., Rusanov, T., Kent, T., Siddique, L.A., and Pomerantz, R.T. (2018). Polymerase θ -helicase efficiently unwinds DNA and RNA-DNA hybrids. *J. Biol. Chem.* **293**, 5259–5269. <https://doi.org/10.1074/jbc.RA117.000565>.
 33. Lemée, F., Bergoglio, V., Fernandez-vidal, A., Machado-silva, A., and Pillaire, M. (2010). DNA polymerase θ up-regulation is associated with poor survival in breast cancer, perturbs DNA replication, and promotes genetic instability. *Proc. Natl. Acad. Sci. USA* **107**. <https://doi.org/10.1073/pnas.0910759107>.
 34. Fernandez-Vidal, A., Guitton-Sert, L., Cadoret, J.C., Drac, M., Schwob, E., Baldacci, G., Cazaux, C., and Hoffmann, J.S. (2014). A role for DNA polymerase θ in the timing of DNA replication. *Nat. Commun.* **5**. <https://doi.org/10.1038/ncomms5285>.
 35. Wang, Z., Song, Y., Li, S., Kurian, S., Xiang, R., Chiba, T., and Wu, X. (2019). DNA polymerase (POLQ) is important for repair of DNA double-strand breaks caused by fork collapse. *J. Biol. Chem.* **294**, 3909–3919. <https://doi.org/10.1074/jbc.RA118.005188>.
 36. Tirman, S., Quinet, A., Wood, M., Meroni, A., Cybulla, E., Jackson, J., Pegoraro, S., Simoneau, A., Zou, L., and Vindigni, A. (2021). Temporally distinct post-replicative repair mechanisms fill PRIMPOL-dependent ssDNA gaps in human cells. *Mol. Cell* **81**, 4026–4040, e8. <https://doi.org/10.1016/j.molcel.2021.09.013>.
 37. Sanjana, N.E., Shalem, O., and Zhang, F. (2014). Improved vectors and genome-wide libraries for CRISPR screening. *Nat. Methods* **11**, 783–784. <https://doi.org/10.1038/nmeth.3047>.
 38. Brinkman, E.K., Chen, T., Amendola, M., and Van Steensel, B. (2014). Easy quantitative assessment of genome editing by sequence trace decomposition. *Nucleic Acids Res.* **42**. <https://doi.org/10.1093/nar/gku936>.
 39. Guzmán, C., Bagga, M., Kaur, A., Westermarck, J., and Abankwa, D. (2014). ColonyArea: an ImageJ plugin to automatically quantify colony formation in clonogenic assays. *PLoS One* **9**, 14–17. <https://doi.org/10.1371/journal.pone.0092444>.
 40. Schneider, C.A., Rasband, W.S., and Eliceiri, K.W. (2012). NIH image to ImageJ: 25 years of image analysis. *Fundam. Digit. Imaging Med.* **9**, 671–675. https://doi.org/10.1007/978-1-84882-087-6_9.
 41. Langmead, B., Trapnell, C., Pop, M., and Salzberg, S.L. (2009). Ultrafast and memory-efficient alignment of short DNA sequences to the human genome. *Genome Biol.* **10**. <https://doi.org/10.1186/gb-2009-10-3-r25>.
 42. Li, W., Xu, H., Xiao, T., Cong, L., Love, M.I., Zhang, F., Irizarry, R.A., Liu, J.S., Brown, M., and Liu, X. (2014). MAGeCK enables robust identification of essential genes from genome-scale CRISPR/Cas9 knockout screens. *Genome Biol.* **15**, 554. <https://doi.org/10.1186/preaccept-1316450832143458>.
 43. Trott, O., and Olson, A.J. (2009). AutoDock Vina: improving the speed and accuracy of docking with a new scoring function, efficient optimization, and multithreading. *J. Comput. Chem.* **32**, 174–182. <https://doi.org/10.1002/jcc>.
 44. Huang, B. (2009). Metapocket: a meta approach to improve protein ligand binding site prediction. *Omi. A J. Integr. Biol.* **13**, 325–330. <https://doi.org/10.1089/omi.2009.0045>.
 45. Michlits, G., Jude, J., Hinterdorfer, M., de Almeida, M., Vainorius, G., Hubmann, M., Neumann, T., Schleiffer, A., Burkard, T.R., Fellner, M., et al. (2020). Multilayered VBC score predicts sgRNAs that efficiently generate loss-of-function alleles. *Nat. Methods* **17**. <https://doi.org/10.1038/s41592-020-0850-8>.
 46. Blencowe, P., Charles, M., Cridland, A., Edkwuru, T., Heald, R., Macdonald, E., McCarron, H., and Rigoreau, L. (2020). Thiazolureas as Anticancer Agents.
 47. Ihlenfeldt, W.D., Bolton, E.E., and Bryant, S.H. (2009). The PubChem chemical structure sketcher. *J. Cheminform.* **1**, 1–9. <https://doi.org/10.1186/1758-2946-1-20>.
 48. Zahn, K.E., Averill, A.M., Aller, P., Wood, R.D., and Doublé, S. (2015). Human DNA polymerase θ grasps the primer terminus to mediate DNA repair. *Nat. Struct. Mol. Biol.* **22**, 304–311. <https://doi.org/10.1038/nsmb.2993>.
 49. Halgren, T.A. (2009). Identifying and characterizing binding sites and assessing druggability. *J. Chem. Inf. Model.* **49**, 377–389. <https://doi.org/10.1021/ci800324m>.
 50. Jackson, D.A., and Pombo, A. (1998). Replicon clusters are stable units of chromosome structure: evidence that nuclear organization contributes to the efficient activation and propagation of S phase in human cells. *J. Cell Biol.* **140**, 1285–1295. <https://doi.org/10.1083/jcb.140.6.1285>.
 51. O'sullivan, J., Mersaoui, S.Y., Poirier, G., and Masson, J.Y. (2021). Assessment of global dna double-strand end resection using brdu-dna labeling coupled with cell cycle discrimination imaging. *J. Vis. Exp.* **2021**, 1–15. <https://doi.org/10.3791/62553>.

STAR★METHODS

KEY RESOURCES TABLE

REAGENT or RESOURCE	SOURCE	IDENTIFIER
Antibodies		
Mouse anti-BRCA1 (D-9)	Santa Cruz	Cat#sc-6954, RRID: AB_626761
Mouse monoclonal anti- α -Tubulin (DM1A)	Cell Signaling Technology	Cat#3873, RRID: AB_1904178
Mouse monoclonal RPA32 (9H8)	Abcam	Cat# ab2175, RRID: AB_302873
Mouse monoclonal Vinculin clone V11F9 (7F9)	Sigma-Aldrich	Cat#MAB3574, RRID: AB_2304338
Peroxidase AffiniPure Goat Anti-Rabbit IgG	Jackson ImmunoResearch	Cat#111-035-144, RRID: AB_2307391
Peroxidase AffiniPure Goat Anti-Mouse IgG	Jackson ImmunoResearch	Cat# 115-035-146, RRID: AB_2307392
Rat monoclonal anti-BrdU BU1/75 (ICR1)	Abcam	Cat#ab6326, RRID: AB_305426
Mouse BrdU Clone B44	BD Biosciences	Cat#347580, RRID: AB_10015219
Cy3 AffiniPure Donkey Anti-Mouse IgG	Jackson ImmunoResearch	Cat#715-165-150, RRID: AB_2340813
Chicken anti-Rat IgG (H + L) Cross-Adsorbed Secondary Antibody, Alexa Fluor™ 488	Invitrogen	Cat#A-21470, RRID: AB_2535873
Goat anti-Mouse IgG (H + L) Cross-Adsorbed Secondary Antibody, Alexa Fluor™ 488	Invitrogen	Cat#A-11001, RRID: AB_2534069
Goat anti-Rat IgG (H + L) Cross-Adsorbed Secondary Antibody, Alexa Fluor™ 555	Invitrogen	Cat#A-21434, RRID: AB_2535855
Goat anti-Rabbit IgG (H + L) Highly Cross-Adsorbed Secondary Antibody, Alexa Fluor™ 568	Invitrogen	Cat#A-11036, RRID: AB_10563566
Rabbit monoclonal anti-RPA70 (EPR3472)	Abcam	Cat#ab79398, RRID: AB_1603759
Mouse monoclonal anti-RPA32 (9H8)	Abcam	Cat#ab2175, RRID: AB_302873
Mouse polyclonal anti-phospho-RPA32(Ser4, Ser8)	Bethyl Laboratories	Cat#A300-245A, RRID: AB_210547
Mouse monoclonal anti-phospho-Histone H2A.X (Ser139) clone JBW301	Sigma-Aldrich	Cat#05-636-1, RRID: AB_2755003
Rabbit monoclonal anti-phospho-Histone H2A.X (Ser139) (20E3)	Cell Signaling Technology	Cat#9718, RRID: AB_2118009
Chemicals, peptides, and recombinant proteins		
Shield-1	Aobious	Cat#AOB1848S
POL θ inhibitor	(Blencowe et al. ²⁰), Enamine	N/A
Mirin	MedChemExpress	Cat# HY-19959
Palbociclib	MedChemExpress	Cat# HY-50767
Olaparib	Selleck Chemicals	Cat#S1060
Etoposide	Selleck Chemicals	Cat# S1225
Ceralasertib	Selleck Chemicals	Cat#HY-19323
JH-RE-06	Axon Medchem	Cat#3002
Nocodazole	Sigma-Aldrich	Cat#M1404
EdU (5-ethynyl-2'-deoxyuridine)	Invitrogen	Cat#11590926
5-Chloro-2-deoxyuridine	Sigma-Aldrich	Cat#C6891
5-Iodo-2-deoxyuridine	Sigma-Aldrich	Cat#I7125

(Continued on next page)

REAGENT or RESOURCE	SOURCE	IDENTIFIER
Continued		
Critical commercial assays		
CellTiter-Glo® Luminescent Cell Viability Assay	Promega	Cat#G7570
QIAmp DNA Blood Mini Kit	Qiagen	Cat#51106
NEBNext® Ultra™ II Q5® Master Mix	New England Biolabs	Cat#M0544S
AMPure XP DNA beads	Beckman Coulter	Cat#A63880
Molecular Probes™ Click-iT™ Plus Alexa Fluor™ 488 Picoyl Azide Toolkit	Molecular Probes	Cat#15403493
Click-iT™ EdU Cell Proliferation Kit for Imaging, Alexa Fluor™ 488 dye	Invitrogen	Cat#C10337
Vectashield® PLUS Antifade Mounting Medium	Vector Laboratories	Cat#H-1900-2
Fluorescence Mounting Medium	Agilent	Cat#S3023
Deposited data		
gRNA sequencing data from genome-wide CRISPR-screen	This paper	NCBI Sequence Read Archive (SRA) PRJNA880040
Experimental models: Cell lines		
Human: hTERT-RPE1 TP53 ^{-/-}	Laboratory of Steve Jackson	N/A
Human: SUM149PT	Laboratory of Steve Jackson	RRID: CVCL_3422
Human: hTERT-RPE1 BRCA1 ^{-/-} TP53 ^{-/-}	Laboratory of Dan Durocher	N/A
Human: HEK-293T	CRUK Cell Facility	RRID: CVCL_0063
Oligonucleotides		
gRNA sequence: CDK6 gRNA #1 5' - GAAGAACGGAGGCCGTTTCG-3'	This paper	N/A
gRNA sequence: CDK6 gRNA #2 5' - GCTGGACTGGAGCAAGACTT-3'	This paper	N/A
gRNA sequence: control 5' - CTCTTCGCTATTACGCCAGC-3'	This paper	N/A
Primers for next generation sequencing library preparation, see Table S2	This paper	N/A
Recombinant DNA		
Plasmid: Toronto human knockout pooled library (TKOv3)	Hart et al. ²⁴	Addgene Plasmid # 90294
Plasmid: psPAX2	Laboratory of Didier Trono	Addgene Plasmid #12260
Plasmid: VSV.G	Laboratory of Tannishtha Reya	Addgene Plasmid #14888
Plasmid: lentiCRISPR v2	Sanjana et al. ³⁷	Addgene Plasmid #52961
Plasmid: DD-Cas9-mVenus	Senturk et al. ²⁹	Addgene Plasmid #90085
Software and algorithms		
TIDE Tracking of Indels by Decomposition	Brinkman et al. ³⁸	https://tide.nki.nl/
Colony Area Plugin	Guzmán et al. ³⁹	https://b2share.eudat.eu/records/39fa39965b314f658e4a198a78d7f6b5
ImageJ	Schneider et al. ⁴⁰	https://imagej.nih.gov/ij/
Incucyte Base Software	Sartorius	N/A
Bowtie	Langmead et al. ⁴¹	http://bowtie-bio.sourceforge.net/
MAGEck	Li et al. ⁴²	https://sourceforge.net/p/mageck/wiki/Home/
FlowJo v10	BD Biosciences	https://www.flowjo.com/
GraphPad Prism 9	GraphPad Software	https://www.graphpad.com/
DAVID Bioinformatics Resources	Huang et al. ^{25,26}	https://david.ncifcrf.gov/

(Continued on next page)

Continued

REAGENT or RESOURCE	SOURCE	IDENTIFIER
Maestro	Schrödinger	https://www.schrodinger.com/products/bioluminate
AutoDock Vina	Trott and Olson ⁴³	https://vina.scripps.edu/
SiteMap	Schrödinger	https://www.schrodinger.com/products/sitemap
MetaPocket	Huang ⁴⁴	https://bioinformatictools.wordpress.com/tag/metapocket/
Olympus ScanR Image Analysis Software	Olympus	N/A
Adobe Illustrator 2022	Adobe	N/A

RESOURCE AVAILABILITY

Lead contact

Additional information and requests for resources and reagents should be directed to and will be fulfilled by the Lead Contact, Joanna I. Loizou (joanna_loizou@hotmail.com).

Materials availability

Cell lines generated in this study are available upon request.

Data and code availability

- CRISPR/Cas9 screen sequencing data have been deposited in the NCBI SRA (PRJNA880040) and are publicly available as of the date of publication. Accession numbers are listed in the [key resource table](#). Microscopy data reported in this paper will be shared by the [lead contact](#) upon request.
- This paper does not report original code. Any additional information required to reanalyze the data reported in this paper is available from the [lead contact](#) upon request.

EXPERIMENTAL MODEL AND SUBJECT DETAILS

Cell lines and culture conditions

RPE1 *TP53*^{-/-} and SUM149PT were kindly provided by Stephen Jackson (Wellcome/Cancer Research UK Gurdon Institute, Cambridge, UK). RPE1 *BRCA1*^{-/-} *TP53*^{-/-} were kindly provided by Daniel Durocher (Lunenfeld-Tanenbaum Research Institute, Toronto, Canada). RPE1 cell lines (female) were grown in Gibco DMEM/F-12 with 10% fetal bovine serum (FBS) and 1% penicillin/streptomycin. SUM149PT (female) were grown in Gibco Ham's F-12 with 5% FBS, 10 mM HEPES, 1 μg/mL hydrocortisone, 5 μg/mL insulin and 1% penicillin/streptomycin. HEK293-T cells (female) were grown in Gibco DMEM with 10% FBS, 10% sodium pyruvate and 1% penicillin/streptomycin. All cells were grown at 3% oxygen and 37°C. Our laboratory conducts regular mycoplasma testing of cultured cells and no mycoplasma contamination of any cell line was detected during this study.

METHOD DETAILS

Plasmids

The Toronto human knockout pooled library (TKOv3) was a gift from Jason Moffat (University of Toronto, Canada Addgene # 90294). For virus production, the psPAX2 (a gift from Didier Trono, EPFL, Switzerland; Addgene plasmid # 12260) and VSV.G (a gift from Tannishtha Reya, UCSD, USA; Addgene plasmid # 14888) packaging plasmids were used. lentiCRISPR v2 was a gift from Feng Zhang (Addgene plasmid # 52961, RRID:Addgene_52961).³⁷ DD-Cas9-mVenus was a gift from Raffaella Sordella (Addgene plasmid # 90085, RRID:Addgene_90085).²⁹

Competitive growth assay

RPE1 *TP53*^{-/-} and RPE1 *BRCA1*^{-/-} *TP53*^{-/-} cells were transduced with DD-Cas9-mVenus encoding either a control or a CDK6 gRNA at an approximate MOI of 0.5. After two days of recovery, the percentage of mVenus-positive cells was measured by flow cytometry to determine initial mVenus levels (day 0) and cells were seeded into 12-well plates together with 200nM Shield-1 (Aobious, #AOB1848S) to induce gRNA expression and DMSO/3μM POLθi. To assess cellular growth kinetics, the percentage of mVenus-positive cells was monitored by flow cytometry every three to four days and normalized to day 0.

Generation of cell lines

For generating CDK6 ko cell lines, gRNAs were designed using <https://www.vbc-score.org/>⁴⁵ and cloned into the pLCV2 backbone, followed by virus production (same procedure as described for TKO v3 virus production) and transduction of cell lines. Transduced cells were selected with puromycin (1.5 μg/ml for RPE1 *TP53*^{-/-}, 20 μg/ml for RPE1 *BRCA1*^{-/-} *TP53*^{-/-} and 1 μg/ml for SUM149PT) and efficiency of ko was determined using TIDE.³⁸ Used gRNA sequences: CDK6#1: 5'-GAAGAACGGAGGCCGTTTCG-3', CDK6#2: 5'-GCTGGACTGGAGCAAGACTT-3' and control: 5'-CTCTTCGCTATTACGCCAGC-3'.

Cell growth assays

Dose-response curves: Dose-response curves were performed in 96-well plates by seeding 400 RPE1 *TP53*^{-/-} or 500 RPE1 *BRCA1*^{-/-} *TP53*^{-/-} cells per well in technical triplicates. For POL*θ*i-etoposide co-treatment dose-response curves, etoposide serial dilutions were added one hour after starting POL*θ*i treatment at indicated concentrations. After four (etoposide)/five (POL*θ*i) days of treatment, cell viability was measured using Cell Titer-Glo (Promega).

Clonogenic survival assays: Clonogenic survival assays for POL*θ*i and olaparib were performed in 6-well plates by seeding cells at low density (for SUM149PT 1000 cells, for RPE1 *TP53*^{-/-} 200 cells and for RPE1 *BRCA1*^{-/-} *TP53*^{-/-} 200 cells per well). On the same day, serial dilutions of POL*θ*i were added. Medium with fresh compound was renewed every three days. After nine and eleven days of treatment, for RPE and SUM149PT respectively, colonies were fixed in 3.7% formaldehyde in PBS and stained with crystal violet solution (0.1% (w/v), 10% EtOH). Colony area was quantified using the ColonyArea plugin in ImageJ and normalized to DMSO.³⁹

Proliferation: Proliferation was assessed with an IncuCyte Live-Cell Analysis Imager (Sartorius). Cellular confluence was monitored over 5 days with images taken every 6 h. Cells were seeded in 48-well plates (for SUM149PT 4000 cells, for RPE1 *TP53*^{-/-} 1000 cells, for RPE *BRCA1*^{-/-} *TP53*^{-/-} 2000 cells per well) and drugs were added immediately after seeding.

Genome-wide CRISPR-Cas9 ko screen

Virus production: The Toronto Knockout (TKO) v3 CRISPR Library virus was produced in a one-production step. HEK-293T cells were seeded in 10cm dishes and transfected 24 h later, with the TKO library plasmid pool, pVSVG and psPAX2 packaging plasmids, using polyethylenimine (PEI). 72 h later, supernatant containing virus was harvested, centrifuged at 2000 rpm for 5 min to remove cell debris and stored at -80°C.

Screen setup: SUM149PT cells were infected with the lentiviral TKOv3 library at a MOI of 0.3 and puromycin-containing medium (0.5 μg/ml) was added the next day to select for transductants. As soon as untransduced control cells were dead (after 5 days of puromycin selection, referred to as "early time point"), 25 million cells were harvested for genomic DNA extraction. After 7 days of puromycin selection, cells were re-seeded with DMSO or a lethal dose (LD) LD90 concentration of POL*θ*i (dynamically adjusted, 2-2.5 μM) and sub-cultured every three days. After 18 days of treatment, 25 million cells per condition were harvested and genomic DNA was extracted using the QIAmp DNA Blood Mini Kit, according to the manufacturer's protocol (referred to as "end time point").

sgRNA amplification and sequencing: Genome-integrated gRNA sequences were amplified by PCR using NEBNext Ultra II Q5 Master Mix. A mixture of P5 forward primers with staggers from 1 to 8 bp and barcoded P7 reverse primers were added in a second round of PCR. The resulting PCR2 product was purified by size-exclusion using magnetic AMPure XP DNA beads (NEB), using a 1:0.95 followed by a 1:1.2 ratio clean-up. Barcoded samples were pooled and sequenced on two flow cells of an Illumina NextSeq 2000 machine using 75 cycles single-read sequencing.

Screen analysis: gRNA sequences were retrieved by trimming all sequences 5' to the adapter sequence (5'-CGAAACACCG-3'). Bowtie (v 2.3.4) was used for alignment and gRNA count.⁴¹ Gene-level depletion scores were calculated using MAGeCK.⁴² End time point samples were compared to early time point samples to analyze depletion of gRNAs targeting essential genes. To identify gene-drug interactions, the POL*θ*i treated endpoint sample was compared to the respective DMSO control.

Immunoblotting

Cell extracts were prepared in RIPA lysis buffer (NEB), supplemented with protease inhibitors (Sigma) and phosphatase inhibitors (Sigma). Immunoblots were performed using standard procedures. Protein samples were separated by sodium dodecyl sulfate-polyacrylamide gel electrophoresis (SDS-PAGE) 3-8% or 4-12% gradient gels (Invitrogen) and subsequently transferred onto PVDF membranes. The following antibodies were used in 5% milk: BRCA1 (1:1000, Santa Cruz, #sc-6954), α -Tubulin (1:1000, CellSignaling, #3873), RPA32 (1:1000, abcam, #ab2175), Vinculin (1:5000, Sigma-Aldrich, #MAB3574). Secondary antibodies (HRP-conjugated goat anti-mouse or anti-rabbit IgG, Jackson Immunochemicals) were used at a 1:5000 dilution. Immunoblots were imaged using a Curix60 (AGFA) table-top processor.

Compounds and inhibitors

POL*θ*i (1-[6-[3-Methyl-4-[(3-methyltetrahydrofuran-3-yl)methoxy]phenyl]pyrazin-2-yl]-3-(6-methyl-3-pyridyl)urea) was custom synthesized by Enamine with 90% purity. MRE11i mirin (#HY-19959), CDK6i Palbociclib (PD 0332991, #HY-50767) and ATRi ceralasertib (AZD6738, #HY-19323) were purchased from MedChemExpress. Etoposide (VP-16, #S1225) and PARPi olaparib (AZD2281, #S1060) were purchased from SelleckChemicals. JH-RE-06 (#3002) was purchased from Axon Medchem. Chemicals were dissolved in DMSO, aliquoted and stored at -20°C.

Flow cytometry

Cell cycle analysis

For determining cell cycle profiles with EdU and DAPI, cells were harvested following a 30-min incubation time with 10 μ M EdU. After one wash in 0.5% BSA in PBS, cells were fixed in 2% paraformaldehyde in PBS for 20 min at room temperature. Cells were washed again in 1x saponin-based permeabilization and wash buffer (Click-iT™ EdU Cell Proliferation Kit for Imaging, Invitrogen) and stained using the Click-iT EdU Alexa Fluor 488 Picolyl Azide Toolkit (Fisher Scientific, #15403493) according to the manufacturer's specifications. DNA was counterstained with DAPI. Cells were washed one more time with 1x saponin based permeabilization and wash buffer, before proceeding to flow cytometry using a BD LSR-Fortessa X-20. Gating and cell cycle analysis were performed using FlowJo (v10). For cell cycle analysis, 20 000 events in the Singlets gate were recorded.

Cell cycle synchronization

Cells were synchronized in mitosis with nocodazole (100 ng/mL, Sigma-Aldrich) for 16 h. To release cells from the mitotic block, cells were washed with warm PBS and then complete medium with either DMSO or 5 μ M POL θ i was added to the wells. At the indicated time points, cells were harvested following a 30-min incubation time with 10 μ M EdU. Cells were prepared as described above for EdU staining.

Gene ontology-term analysis

DAVID Bioinformatics Resources functional annotation online-tool was used for GO-term analysis of genes represented by the top enriched gRNAs ($p < 0.005$), using "Uniprot Biological Process" as functional annotation term.^{25,26} The gene list was treated as an unordered query.

Identification and scoring of a POL θ i binding pocket in the POL θ polymerase domain

The chemical structures of POL θ inhibitors were extracted from two patents.^{20,46} In these patents, the inhibitory potency of 342 compounds was measured on the polymerase domain of POL θ . In the following, compounds of both patents will be referred to as POL θ inhibitors. The strongest inhibitor, 25A-90, is referred to in the singular (POL θ inhibitor). The thiazoleurea compounds⁴⁶ are referred to as 24A-xxx followed by the ID number (e.g. 24A-116) and the heterocyclic substituted urea compounds as 25A-xxx (e.g. 25A-92).²⁰ POL θ inhibitors for docking analysis were generated using PubChem Sketcher.⁴⁷ The structure of the POL θ polymerase domain was obtained from the RCSB Protein Database (PDB entry 4X0P).⁴⁸ Nucleotides, DNA, and solvent were deleted from the structure and the protein was prepared using Maestro (Schrödinger Release 2022-1: BioLuminate, Schrödinger, LLC, New York, NY, 2021.) Three independent methods were used to identify possible binding pockets, namely blind docking with AutoDock Vina,⁴³ binding site identification with SiteMap⁴⁹ and the consensus pocket identification approach MetaPocket.⁴⁴ AutoDock Vina 1.1 was used to perform the blind docking experiment in which buriedness was set to zero, exhaustiveness level to 8, and the number of binding modes to 9. The dimensions of the grid box were scaled to include the complete protein. Additionally, SiteMap and MetaPocket were used to identify potential binding sites. The results were analyzed using the SiteScore and size values calculated by SiteMap and the Z score calculated by MetaPocket. Binding hypotheses were further analyzed by their ability to generate reasonable hypotheses for the activity cliff pairs (25A-104, 25A-150), (25A-69, 25A-54), and (25A-213, 25A-90).

DNA fiber assay

Asynchronous cells were pulse labeled with 25 μ M CldU (Sigma-Aldrich, #C6891) for 20 min, washed twice with warm PBS and then labeled with 250 μ M IdU (Sigma-Aldrich, #I7125) for 20 min. POL θ i (5 μ M) was added 90 min before the labeling and was present for the entire labeling time. Cells were trypsinized, counted and resuspended at a final concentration of $1-2 \times 10^3$ cells/ μ L. Two μ L of cell suspension were lysed on a clean glass slide with 8 μ L of MES lysis buffer (500 mM MES pH 5.6, 0.5% SDS, 50 mM EDTA, 100 mM NaCl) for 7 min, then the slide was tilted 15° to allow the DNA to spread. Slides were air dried for 30 min, fixed in freshly prepared acetic acid/methanol (1:3) for 10 min, air dried and store at 4°C overnight. Slides were rehydrated with PBS 1X for 5 min, DNA was denatured with 2.5 M HCl for 80 min, slides were washed several times with PBS and blocked in blocking solution (5% BSA, 0.2% Triton X-100 in PBS) for 20 min. Slides were incubated with primary antibody mix of anti-BrdU (abcam, #ab6326, 1:100) which recognizes CldU, and anti-BrdU (BD biosciences, #347580, 1:50) which recognizes IdU in blocking solution for 90 min at 37°C in a humid chamber. After incubation, slides were washed once with 0.1% Tween in PBS and twice with PBS for 3 min each. Slides were incubated with secondary antibody mix of donkey anti-mouse CY3 (Jackson ImmunoResearch, #715-165-150) and chicken anti-rat Alexa 488 (ThermoFisher, #A-21470) in blocking solution for 45 min at 37°C degrees in a humid chamber. Slides were washed 3 times in PBS, air dried, mounted in vectashield plus (Vector labs) and stored at 4°C until image acquisition. Images were acquired with an Olympus Upright BX61 fluorescence microscope with a 60X oil immersion objective 1.35 NA. According to the fiber density between 5 and 10 images were captured per condition and at least 200 fibers were measured using ImageJ software version 2.3.0/1.53f.⁴⁰ For fork speed experiments, the conversion factor used was 1 μ m = 2.59kb.⁵⁰

S1 nuclease assay

The S1 assay was conducted as previously described.⁵ Briefly, cells were pulse labeled with 25 μ M CldU (Sigma-Aldrich, #C6891) for 20 min, washed twice with warm PBS and then labeled with 250 μ M IdU (Sigma-Aldrich, #I7125) for 40 min. POL θ i (5 μ M) was added

90 min before labeling and was present during the whole labeling procedure. Cells were washed once with PBS and then permeabilized with CSK100 buffer (100 mM NaCl, 10 mM PIPES pH 6.8, 3mM MgCl₂, 300 mM sucrose, Triton 0.5% X-100) for 10 min at room temperature. Exposed nuclei were washed once with S1 buffer (30 mM Sodium acetate pH 4, 2 mM Zinc sulfate, 50 mM NaCl, 5% glycerol) and then incubated with 10 U/mL of S1 nuclease (Sigma-Aldrich, #N5661) in S1 buffer for 20 min at 37°C. Nuclei were scraped in 1 mL of PBS 0.1% BSA, centrifugated 5 min at 7000 rpm and resuspend in PBS to a final concentration of 1-2x10³ nuclei/μL. DNA was spread and stained as is the DNA fiber assay.

Immunofluorescence and imaging

ssDNA: Cells were grown on 12mm glass coverslips in 10 μM BrdU for 48 h, followed by the indicated treatments as described. After treatment, cells were washed in PBS and pre-extracted with Pre-Extraction buffer (10mM PIPES, 100mM NaCl, 3mM MgCl₂, 1mM EGTA, 0.5% Triton X-100 and 300mM Sucrose) for 10 min at 4°C, followed by Cytoskeleton Stripping Buffer B (10mM Tris pH 7.5, 10mM NaCl, 3mM MgCl₂, 1% Tween 20, 0.5% sodium deoxycholate) for additional 10 min at 4°C.⁵¹ Cells were then washed in PBS, fixed using 2% formaldehyde for 15 min at room temperature and permeabilization was carried out for 10 min in 0.5% Triton X-100 in PBS. Cells were incubated 1 h in blocking buffer and stained with primary antibodies against BrdU (Abcam, #ab6326) at 37°C for 1 h. Cells were washed and incubated with secondary antibodies (Alexa Fluor 555) for 1 h at room temperature. After washing, cells were incubated with DAPI (1 ug/ml) and mounted onto glass slides using DAKO Fluorescent Mounting Medium (Agilent Technologies S3023). Images were visualized by confocal microscopy (LSM-700 Zeiss) at a constant exposure time in each experiment. The number of BrdU foci per nucleus was measured with Cell Profiler software version 4.2.1 from the Broad Institute.

High content-microscopy: Cells were grown in 96-well optically-clear cyclic olefin bottom plates (PhenoPlate #6055300, PerkinElmer), pre-extracted, fixed and permeabilized as described above. Cells were labeled with primary antibodies (RPA70, 1:500, abcam, #ab79398, RPA 32/2, abcam, 1:500, #ab2175, phospho-RPA32 (Ser4,Ser8), 1:500, Bethyl Laboratories, #A300-245A, phospho-histone-H2A.X, 1:1000, Sigma-Aldrich, #05-636-l, anti-phospho-histone-H2A.X/γ-H2AX 20E3, 1:400, Cell Signaling, #9718) overnight at 4°C. Cells were washed three times in PBS-Tween 0.1% and incubated with appropriate secondary antibodies for 1 h at room temperature. Automated multichannel wide-field microscopy for quantitative image-based cytometry (QIBC) was performed on an Olympus IXplore SpinSR inverted research microscope using 40X magnification (Olympus, Life Science Solutions). Images were analyzed with the Olympus ScanR Image Analysis Software (Olympus OSIS Life Science Solutions, version 3.3), a dynamic background correction was applied, and nuclei segmentation was performed using an edge-based object detection module based on the DAPI signal. Mean intensities and scatterplots were displayed using Python version 3.

QUANTIFICATION AND STATISTICAL ANALYSIS

Statistical analysis

Statistical tests were performed as indicated in the figure legends to determine statistical significance and were performed using GraphPad Prism (Version 9.0). In all cases, ns: not significant ($p > 0.05$), *: $p < 0.05$, **: $p < 0.01$, ***: $p < 0.001$ and ****: $p < 0.0001$.

Figure legends indicate the number of replicates for each experiment and if data are represented as mean or median ±SD.